Computers and Structures 88 (2010) 991–1001

Contents lists available at ScienceDirect

Computers and Structures

journal homepage: www.elsevier.com/locate/compstruc

Free vibration analysis of rotating Euler beams at high angular velocity

Chih Ling Huang [a], Wen Yi Lin [b], Kuo Mo Hsiao [a,*]

[a] Department of Mechanical Engineering, National Chiao Tung University, Hsinchu, Taiwan
[b] Department of Mechanical Engineering, De Lin Institute of Technology, Tucheng, Taiwan

ARTICLE INFO

Article history:
Received 10 November 2009
Accepted 7 June 2010
Available online 14 July 2010

Keywords:
Rotating beam
Vibration
Natural frequency
Power series solution
Frequency veering

ABSTRACT

The natural frequency of the flapwise bending vibration, and coupled lagwise bending and axial vibration is investigated for the rotating beam. A method based on the power series solution is proposed to solve the natural frequency of very slender rotating beam at high angular velocity. The rotating beam is subdivided into several equal segments. The governing equations of each segment are solved by a power series. Numerical examples are studied to demonstrate the accuracy and efficiency of the proposed method. The effect of Coriolis force, angular velocity, and slenderness ratio on the natural frequency of rotating beams is investigated.

1. Introduction

Rotating beams are often used as a simple model for propellers, turbine blades, and satellite booms. The free vibration frequencies of rotating beams have been extensively studied [1–19]. Rotating beam differs from a non-rotating beam in having additional centrifugal force and Coriolis effects on its dynamics. The lagwise bending and axial vibration are coupled due to the Coriolis effects [8,15,18]. However, most studies neglected the Coriolis effects in the literature. It is well known that the beam sustains a steady state axial deformations (time-independent displacement) induced by constant rotation [20]. For the rotating uniform beam as shown in Fig. 1, the maximum steady axial strain occurs at the root of the beam and may be expressed as [15] $\varepsilon_{\max} = \bar{k}^2(R/L + 0.5)$, where $\bar{k} = \Omega L\sqrt{\rho/E}$ is a dimensionless angular velocity, R is the radius of the hub, L, ρ, and E are the length, density, and Young's modulus of the beam, respectively, Ω is the angular velocity of the hub. In practice, rotating structures are designed to operate in the elastic range of the materials. Thus, the allowable value of the maximum steady axial strain for the rotating beam should be smaller than the yield strain, which is much smaller than unity for most engineering material. In this sense, if the maximum steady axial strain is close to the yield strain, the corresponding angular velocity may be called high angular velocity. However, as mentioned in [15], the magnitudes of the steady state axial strain induced by the centrifugal force and the corresponding angular velocity are not checked in most literature. The dimensionless angular velocity used in most literature is $\bar{\eta}\bar{k}$, where $\bar{\eta}$ is the slenderness ratio of the beam. The difference of the maximum steady axial strains corresponding to the same value of $\bar{\eta}\bar{k}$ may be remarked for rotating beams with different slenderness ratio. Thus, the maximum steady axial strains corresponding to some angular velocity considered in many literatures are even larger than unity for rotating beam with small slenderness ratio, but are much smaller than the yield strain of most engineering material for very slender beam. In this study, if the maximum steady axial strain is much smaller than the yield strain, the corresponding angular velocity is regarded as low angular velocity. To the authors' knowledge, the study of the natural frequency for very slender rotating beam at high angular velocity is rather rare in the literature. The objective of this paper is to investigate the natural frequencies of the flapwise bending vibration, and coupled lagwise bending and axial vibration for very slender rotating Euler beam at high angular velocity using power series solution. However, the rotating beams with different slenderness ratio at different angular velocities are also investigated.

A number of methods based on the power series solution have been developed for determination of natural frequencies and mode shapes of rotating beams [2,6,9–19]. However, only the uncoupled bending vibration was considered in most methods based on the power series solution. It was asserted that only one single segment is needed for power series solution to obtain any modal frequency or mode shape for uniform beams or uniformly tapered beams in [17]. A similar statement was given in [18]. However, no results for slender rotation beams at high angular velocity were given in [17,18]. The assertion given in [17,18] may be correct if a computer can retain infinite number of significant digits to represent the result of an operation. However, any computer can only retain a finite number of significant digits to represent the result of an operation. The accuracy of the calculated natural frequency

* Corresponding author. Tel.: +886 3 5712121x55107; fax: +886 3 5720634.
E-mail address: kmhsiao@mail.nctu.edu.tw (K.M. Hsiao).

0045-7949/$ - see front matter © 2010 Elsevier Ltd. All rights reserved.
doi:10.1016/j.compstruc.2010.06.001

Nomenclature

A	cross-section area of rotating beam
E	Young's modulus
F_1	force in X_1 direction
F_3	force in X_3 direction
I	principal second moment of cross-section area
k	$\bar{k}/N$
$\bar{k}$	dimensionless angular velocity of the hub
K	$\overline{K}/N$
$\overline{K}$	dimensionless natural frequency of rotating beam
l	length of each segment
L	length of rotating beam
M	moment about negative X_2 axis
N	number of segments
$\bar{r}$	dimensionless radius of rotating hub
$\mathbf{r}$	position vector
$\ddot{\mathbf{r}}$	second time derivative of $\mathbf{r}$
R	radius of the hub
t	time
u	time dependent infinitesimal displacements in X_1 direction
U	dimensionless u
u_s	steady state axial deformations
w	time dependent infinitesimal displacements in X_3 direction
W	dimensionless w
β	setting angle of rotating beam
ε	axial strain
$\varepsilon_{\max}$	maximum steady axial strain of rotating beam
η	$\bar{\eta}/N$
$\bar{\eta}$	slenderness ratio of rotating beam
θ	rotation of beam cross-section
ω	natural frequency of rotating beam
Ω	angular velocity of hub

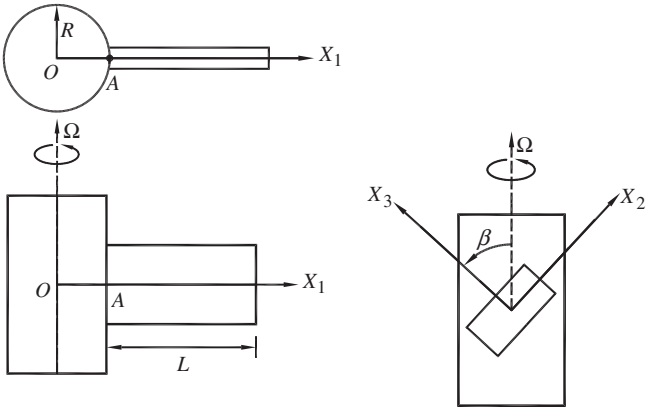

Fig. 1. A rotating Euler beam.

depends on the precision with which the computing facility operates, and a great number of terms in the power series solution does not necessarily result in a more accurate solution [12]. The authors use the power series method proposed in [15] and double precision computation to calculate the natural frequencies for slender rotating beams at high angular velocity. It is found that the rate of convergence of the power series solution is slower at higher angular velocity and the computation fail to converge when the angular velocity is higher than some value. In [12], it is found that to calculate the frequencies for rotating beam at high centrifugal tension using one segment and quadruple precision computation failed for some case due to arithmetic overflow. The failure may be attributable to the accuracy lost caused by the insufficient precision used in computation. It seems that the rate of convergence of the power series solution decreases and the degree of accuracy lost of the power series solution in computation increases with the increase of the dimensionless angular velocity $\bar{k}$. The power series solution using one segment with quadruple precision computation may be still not enough to get the frequencies for slender rotating beams at very high angular velocity. However, using quadruple or higher precision computation may be impractical. To alleviate the aforementioned numerical difficulties, in this study, a practical method based on the power series solution is proposed to solve the natural frequency of slender rotating beam at very high angular velocity.

In this study, the equations of motion for rotating Euler beam are derived by the d'Alembert principle and the virtual work principle. In order to capture all inertia effect and coupling between extensional and flexural deformation, the consistent linearization [21–23] of the fully geometrically non-linear beam theory [22,23] is used in the derivation. The governing equations for linear vibration of rotating beam are two coupled linear ordinary differential equations with variable coefficients. The rotating beam is subdivided into several equal segments. The solution of each segment is expressed as a power series with six independent coefficients. Substituting the power series solution of each segment into the corresponding boundary conditions at two end nodes of the rotating beam and the continuity conditions at common node between two adjacent segments, a set of homogeneous equations can be obtained. The natural frequencies may be determined by solving the homogeneous equations using the bisection method.

The dimensionless angular velocity corresponding to each segment is $\bar{k}/N$, where N is the number of segment. Subdividing the rotating beam into more segments can make the value of dimensionless angular velocity in the power series solution smaller. We believe that when the value of dimensionless angular velocity in the power series solution decrease, the rate of convergence of power series solution will increase, the accuracy lost in computation will decrease, and double precision computation will be sufficient to obtain natural frequency with high accuracy for slender rotating beams at very high angular velocity. This belief will be examined through numerical examples in the paper. Numerical examples are studied to investigate the effect of Coriolis force, rotary inertia, angular velocity, hub radius and slenderness ratio on the natural frequency of rotating beams. The frequency veering phenomenon [24] induced by the Coriolis force and the centrifugal force are also investigated.

2. Formulation

2.1. Description of problem

Consider a uniform Euler beam of length L rigidly mounted on the periphery of rigid hub with radius R rotating about its axis fixed in space at a constant angular velocity Ω as shown in Fig. 1. The deformation displacements of the beam are defined in a rotating rectangular Cartesian coordinate system which is rigidly tied to the hub. The origin of this coordinate system is chosen to be the intersection of the centroid axes of the hub and the undeformed beam. The X_1 axis is chosen to coincide with the centroid axis of the undeformed beam, and the X_2 and X_3 axes are chosen to be

the principal directions of the beam cross-section at the undeformed state. The angular velocity of the hub may be given by

$$\Omega = \{\, 0 \quad \Omega \sin\beta \quad \Omega \cos\beta \,\} \tag{1}$$

where the symbol $\{\,\}$ denotes a column matrix, which is used through the paper, β, the angle between the hub axis and the X_3 axis, is the setting angle of the beam.

Here it is assumed that the beam is only deformed in the X_1–X_3 plane. As mentioned in [15], the flapwise and lagwise bending motions are coupled for setting angles other than $\beta = 0^\circ$ and 90°. Thus, only $\beta = 0^\circ$ and 90° are considered in this study. When $\beta = 0^\circ$ and 90°, bending vibrations are flapwise and lagwise, respectively. It is well known that the beam sustains a steady state axial deformations (time-independent displacement) induced by constant rotation [20]. In this study, the vibration (time-dependent displacement) of the beam is measured from the position of the steady state axial deformation, and only infinitesimal free vibration is considered. Here the engineering strain and stress are used for the measure of the strain and stress. It is assumed that the strains are small and the stress–strain relationships are linear.

2.2. Kinematics of Euler beam

Let P (see Fig. 2) be an arbitrary point in the rotating beam, and Q be the point corresponding to the beam cross-section of P on the centroid axis. The position vector of point P in the undeformed and deformed configurations may be expressed as

$$\mathbf{r}_0 = \{\, R + x \quad y \quad z \,\} \tag{2}$$

$$\mathbf{r} = \{\, R + x + \bar{u}(x,t) - z\sin\theta \quad y \quad w(x,t) + z\cos\theta \,\} \tag{3}$$

$$\bar{u}(x,t) = u_s(x) + u(x,t) \tag{4}$$

where t is time, $u_s(x)$ is the steady state axial deformations induced by constant rotation, $u(x,t)$ and $w(x,t)$ are the infinitesimal displacements of point Q in the X_1 and X_3 directions, respectively, caused by the free vibration, $\theta = \theta(x,t)$ is the infinitesimal angle of rotation of the cross-section passing through point Q about the negative X_2 axis, caused by the free vibration.

From Eq. (3) and the definition of engineering strain [25,26], making use of the assumption of small strain, and using the approximation $\sin\theta \approx \theta \approx w_{,x}$ and $\cos\theta \approx 1$, the engineering strain in the Euler beam may be approximated by

$$\varepsilon = \bar{u}_{,x} + \frac{1}{2}w_{,x}^2 - z w_{,xx} \tag{5}$$

2.3. Equations of motion

The equations of motion for rotating Euler beam are derived by the d'Alembert principle, the virtual work principle and the consistent first order linearization of the fully geometrically non-linear beam theory [22,23]. Fig. 3 shows a portion of the deformed centreline of the beam. Here the generalized displacements are chosen to be $\bar{u}$, w, and θ defined in Eq. (3). Note that the approximation $\theta \approx w_{,x}$ is used in this study. The corresponding generalized forces are F_1, F_3, and M, the forces in X_1, X_3 directions, and moment about negative X_2 axis. F_{1j}, F_{3j}, and M_j ($j = a, b$) in Fig. 3 denote the values of F_1, F_3, and M at section j.

For linear elastic material, the virtual work principle may be written as

$$\delta W_{ext} = \delta W_{int} \tag{6}$$

$$\delta W_{ext} = (F_1\delta\bar{u} + F_3\delta w + M\delta\theta)\big|_a^b = \int_a^b \frac{d}{dx}(F_1\delta\bar{u} + F_3\delta w + M\delta\theta)dx \tag{7}$$

$$\delta W_{int} = E\int_{V_{ab}} \delta\varepsilon^t \varepsilon\, dV + \rho\int_{V_{ab}} \ddot{\mathbf{r}}^t \delta\mathbf{r}\, dV \tag{8}$$

where δW_{ext} and δW_{int} are the virtual work of the external forces and the internal stresses, respectively, $()|_a^b$ is the value of $(\,)$ at section b minus the value of $(\,)$ at section a, $\delta\bar{u}$, δw and $\delta\theta$ are the virtual displacements, $\delta\varepsilon$ is the variation of ε given in Eq. (5), E is Young's modulus, V_{ab} is the volume of the undeformed beam between section a and section b. The differential volume dV may be expressed as $dV = dA\,dx$, where dA is the differential cross-section area of the beam, ρ is the density, $\delta\mathbf{r}$ is the variation of $\mathbf{r}$ given in Eq. (3), and $\ddot{\mathbf{r}} = d^2\mathbf{r}/dt^2$. The symbol $\dot{()}$ denotes differentiation with respect to time t. The derivations and explicit forms of $\delta\varepsilon$, $\delta\mathbf{r}$, and $\ddot{\mathbf{r}}$ are provided in the Appendix.

The exact expression of δW_{int} may be very complicated. However, due to the assumption of infinitesimal vibration, the quantities u, w, and θ defined in Eqs. (3) and (4), and their derivatives with respect to x and t are all infinitesimal quantities. For linear vibration analysis only the terms up to the first order of infinitesimal quantities are required. All terms up to the first order of infinitesimal quantities in δW_{int} are retained. Note that the steady state

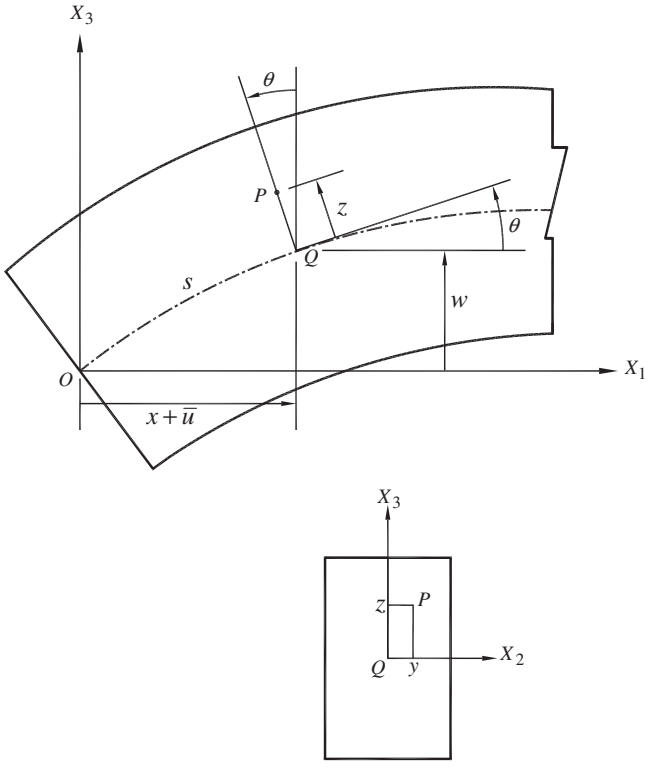

Fig. 2. Kinematics of deformed Euler beam.

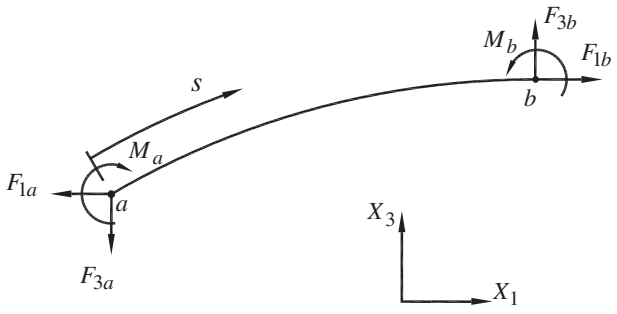

Fig. 3. Free body of a portion of deformed beam.

axial deformations $u_s(x)$ in Eq. (4) and its derivatives with respect to x are small finite quantities, not infinitesimal quantities, and are all retained as zeroth order terms of infinitesimal quantities.

Substituting Eqs. (5), (A.1), (A.2), and (A.5) into Eq. (8), using $\int_A z\,dA = 0$, $\int_A yz\,dA = 0$, and retaining all terms up to the first order of infinitesimal quantities, and then substituting Eqs. (7) and (8) into Eq. (6), and equating the terms in both sides of Eq. (6) corresponding to the same generalized virtual displacements, one may obtain

$$F_{1,x} = \rho A[\ddot{u} + 2\Omega\dot{w}\sin\beta - \Omega^2(R + x + \bar{u})] \tag{9}$$

$$F_{3,x} = \rho A(\ddot{w} - 2\Omega\dot{u}\sin\beta - \Omega^2 w\sin^2\beta) \tag{10}$$

$$F_3 + M_{,x} = EA\bar{u}_{,x}w_{,x} + \rho I(\ddot{w}_{,x} - \Omega^2 w_{,x}\cos^2\beta) \tag{11}$$

$$M = EIw_{,xx} \tag{12}$$

$$F_1 = EA\bar{u}_{,x} \tag{13}$$

where $I = \int_A z^2\,dA$ is the principal second moment of the cross-section area. Eqs. (9)–(11) are equations of motion and Eqs. (12) and (13) are constitutive equations.

From Eqs. (9) and (13), and Eqs. (10)–(12), one may obtain

$$EA\bar{u}_{,xx} = \rho A[\ddot{u} + \underline{2\Omega\dot{w}\sin\beta} - \Omega^2(R + x + \bar{u})] \tag{14}$$

$$EIw_{,xxxx} = EA(\bar{u}_{,x}w_{,x})_{,x} - \rho A(\ddot{w}\underline{-2\Omega\dot{u}\sin\beta} - \Omega^2 w\sin^2\beta) + \rho I(\underline{\ddot{w}_{,xx} - \Omega^2 w_{,xx}\cos^2\beta}) \tag{15}$$

where the single underlined terms are Coriolis force terms and the double underlined terms are rotary inertia terms. When $\beta = 0^\circ$ and 90°, bending vibrations are flapwise and lagwise. respectively. The flapwise bending vibration and axial vibration are not coupled. However, due to the effect of the Coriolis force, the lagwise bending vibration and axial vibration are coupled.

The boundary conditions for a rotating Euler beam with fixed end at $x = 0$ and free end at $x = L$ are given by

$$\begin{aligned} &u_s(0) = u(0,t) = 0, \quad w(0,t) = 0, \quad w_{,x}(0,t) = 0 \\ &F_1(L,t) = 0, \quad M(L,t) = 0, \quad F_3(L,t) = 0 \end{aligned} \tag{16}$$

2.4. Steady state axial deformation

For the steady state axial deformations, $\bar{u}(x,t) = u_s(x)$, $u(x,t) = w(x,t) = 0$. Thus Eqs. (14)–(16) can be reduced to

$$EAu_{s,xx} = -\rho A\Omega^2(R + x + u_s) \tag{17}$$

$$u_s(0) = 0, \quad u_{s,x}(L) = 0 \tag{18}$$

Let

$$\bar{k} = \Omega L\sqrt{\rho/E} \tag{19}$$

where $\bar{k}$ is a dimensionless angular velocity. If $\bar{k} \ll 1$, the steady state axial deformation $u_s(x)$, which satisfies Eqs. (17) and (18), may be approximated by [15]

$$u_s(x) = \frac{\bar{k}^2}{L^2}\left(\frac{-x^3}{6} - \frac{Rx^2}{2} + \frac{L^2x}{2} + RLx\right) \tag{20}$$

The maximum value of the steady state axial strain corresponding to the axial deformation given in Eq. (20) occurs at the root of the beam and may be expressed as

$$\varepsilon_{\max} = u_{s,x}(L) = \bar{k}^2(\bar{r} + 0.5) \tag{21}$$

$$\bar{r} = \frac{R}{L} \tag{22}$$

where $\bar{r}$ is a dimensionless radius of the rotating hub, and R is the radius of the rotating hub. In practice, $\varepsilon_{\max}$ should not be larger than the yield strain. For most engineering materials, the yield strain is much smaller than unit. In this study, if the maximum steady axial strain is close to the yield strain, the corresponding angular velocity is called high angular velocity.

2.5. Free vibration

The vibration of the beam is measured from the position of the steady state axial deformation. To obtain the natural frequency of the rotating beam, the beam is subdivided into N equal segments. The length for each segment is $l = L/N$. For convenience, the following nondimensional variables are used:

$$\xi_m = \frac{x - x_m}{l} - \frac{1}{2}, \quad U_m = U(\xi_m) = \frac{u}{l}, \quad W_m = W(\xi_m) = \frac{w}{l}, \quad k = \frac{\bar{k}}{N}, \quad \eta = \frac{\bar{\eta}}{N} \tag{23}$$

$$\bar{\eta} = \sqrt{\frac{AL^2}{I}} \tag{24}$$

where $x_m \leqslant x \leqslant x_{m+1}$, $x_m = (m-1)l$, $m = 1, 2, \ldots, N$, m denotes the mth segment, $\bar{k}$ is defined in Eq. (19), and $\bar{\eta}$ is the slenderness ratio of the beam.

Note that the segment index m will hereafter be dropped for simplicity of notation unless clarity is lost.

From Eqs. (4), (14), (15), (19), (20), (23), and (24), the dimensionless governing equations of free vibration for segment m may be expressed as

$$U_{,\xi\xi} - \frac{\rho l^2}{E}(\ddot{U} - \Omega^2 U + \underline{2\Omega\dot{W}\sin\beta}) = 0 \tag{25}$$

$$W_{,\xi\xi\xi\xi} - \eta^2(U_{s,\xi}W_{,\xi})_{,\xi} - \frac{\rho l^2}{E}(\underline{\ddot{W}_{,\xi\xi} - \Omega^2 W_{,\xi\xi}\cos^2\beta}) - \frac{\rho A l^4}{EI}(\underline{2\Omega\dot{U}\sin\beta} - \ddot{W} + \Omega^2 W\sin^2\beta) = 0$$

$$U_{s,\xi} = -k^2(0.5\xi^2 + r_m\xi - 0.5Q_m^2 - Q_m r_m) \tag{26}$$

$$r_m = r + m - \frac{1}{2}, \quad Q_m = N - m + \frac{1}{2}, \quad r = N\bar{r} \tag{27}$$

We shall seek a solution of Eq. (25) in the form

$$\mathbf{U}(\xi,t) = [\mathbf{U}_R(\xi) + i\mathbf{U}_I(\xi)]e^{i\omega t} \tag{28}$$

$$\mathbf{U}(\xi,t) = \{U, W\}, \quad \mathbf{U}_R(\xi) = \{U_R, W_R\}, \quad \mathbf{U}_I(\xi) = \{U_I, W_I\} \tag{29}$$

where $i = \sqrt{-1}$, and ω is the natural frequency to be determined. For convenience, the following nondimensional variables are used:

$$K = \overline{K}/N \tag{30}$$

$$\overline{K} = \omega L\sqrt{\rho/E} \tag{31}$$

where $\overline{K}$ is a dimensionless natural frequency of the rotating beam.

Introducing Eq. (28) into Eq. (25), it is observed that $U_I = U_R$ and $W_R = -W_I$. Thus only U_R and W_I are solved in this study and the corresponding governing equations are given by

$$U_{R,\xi\xi} + aU_R + bW_I = 0 \tag{32}$$

$$W_{I,\xi\xi\xi\xi} + (c\xi^2 + d\xi + e)W_{I,\xi\xi} + (2c\xi + d)W_{I,\xi} - \eta^2 bU_R - fW_I = 0$$

$$a = K^2 + k^2, \quad b = 2Kk\sin\beta, \quad c = 0.5\eta^2k^2, \quad d = \eta^2k^2r_m \tag{33}$$

$$e = K^2 + k^2\cos^2\beta - \eta^2k^2(0.5Q_m^2 + r_mQ_m), \quad f = \eta^2(K^2 + k^2\sin^2\beta),$$

2.6. Power series solution

The solution of Eq. (32) can be expressed as a power series in the independent variable ξ:

$$\mathbf{A}(\xi)=\begin{Bmatrix}U_R\\W_I\end{Bmatrix}=\sum_{n=0}^{\infty}\begin{Bmatrix}C_n\\D_n\end{Bmatrix}\xi^n=\sum_{n=0}^{\infty}\mathbf{C}_n\xi^n \tag{34}$$

where C_n, D_n are undetermined coefficients.

Substituting Eq. (34) into Eq. (32) and equating coefficients of like power of ξ, we obtain the recurrence formula

$$\mathbf{C}_n=\sum_{j=1}^{4}\mathbf{A}_n^j\mathbf{C}_{n-j},\quad n\geqslant 4 \tag{35}$$

$$C_2=-\frac{1}{2}\{a\quad b\}^t\mathbf{C}_0,\quad C_3=-\frac{1}{6}\{a\quad b\}^t\mathbf{C}_1 \tag{36}$$

$$\begin{aligned}\mathbf{A}_n^1&=\mathbf{0}_{2\times 2},\quad \mathbf{A}_n^2=\frac{-1}{n(n-1)}\begin{bmatrix}a&b\\0&e\end{bmatrix},\\ \mathbf{A}_n^3&=\frac{-(n-3)}{n(n-1)(n-2)}\begin{bmatrix}0&0\\0&d\end{bmatrix}\\ \mathbf{A}_n^4&=\frac{1}{n(n-1)(n-2)(n-3)}\begin{bmatrix}0&0\\\eta b&f-c(n-3)(n-4)\end{bmatrix}\end{aligned} \tag{37}$$

From Eq. (35), It can be seen that only C_0, D_0, C_1, D_1, D_2 and D_3 are independent constants in Eq. (34), and $\mathbf{C}_n$ ($n\geqslant 4$) can be rewritten as

$$\mathbf{C}_n=(\mathbf{Y}_0^n+\mathbf{Y}_2^n\mathbf{D}_a)\mathbf{C}_0+(\mathbf{Y}_1^n+\mathbf{Y}_3^n\mathbf{D}_b)\mathbf{C}_1+D_2\mathbf{Y}_2^n\mathbf{e}_2+D_3\mathbf{Y}_3^n\mathbf{e}_2,\quad n\geqslant 4 \tag{38}$$

$$\mathbf{Y}_i^n=\sum_{j=1}^{4}\mathbf{A}_n^j\mathbf{Y}_i^{n-j},\quad i=0,1,2,3 \tag{39}$$

$$\mathbf{Y}_i^j=\begin{cases}\mathbf{I} & \text{if } i=j\\ \mathbf{0} & \text{if } i\neq j\end{cases},\quad i,j=0,1,2,3 \tag{40}$$

$$\mathbf{D}_a=\frac{-1}{2}\begin{bmatrix}a&b\\0&0\end{bmatrix},\quad \mathbf{D}_a=\frac{-1}{6}\begin{bmatrix}a&b\\0&0\end{bmatrix},\quad \mathbf{e}_2=\begin{Bmatrix}0\\1\end{Bmatrix} \tag{41}$$

where $\mathbf{I}$ and $\mathbf{0}$ are unit matrix and zero matrix of order 2×2, respectively.

Substituting Eq. (38) into Eq. (34), Eq. (34) can be rewritten as

$$\mathbf{A}(\xi)=\mathbf{E}(\xi)\mathbf{C} \tag{42}$$

$$\mathbf{E}(\xi)=[\mathbf{E}_1\quad \mathbf{E}_2\quad \mathbf{E}_3] \tag{43}$$

$$\begin{aligned}\mathbf{E}_1&=\mathbf{I}+\xi^2\mathbf{D}_a+\sum_{n=4}^{\infty}\xi^n(\mathbf{Y}_0^n+\mathbf{Y}_2^n\mathbf{D}_a),\\ \mathbf{E}_2&=\xi\mathbf{I}+\xi^3\mathbf{D}_b+\sum_{n=4}^{\infty}\xi^n(\mathbf{Y}_1^n+\mathbf{Y}_3^n\mathbf{D}_b)\end{aligned}$$

$$\mathbf{E}_3=[\mathbf{E}_4\mathbf{e}_2\quad \mathbf{E}_5\mathbf{e}_2],\quad \mathbf{E}_4=\xi^2\mathbf{I}+\sum_{n=4}^{\infty}\xi^n\mathbf{Y}_2^n,\quad \mathbf{E}_5=\xi^3\mathbf{I}+\sum_{n=4}^{\infty}\xi^n\mathbf{Y}_3^n$$

$$\mathbf{C}=\{C_0\quad D_0\quad C_1\quad D_1\quad D_2\quad D_3\} \tag{44}$$

where $\mathbf{E}(\xi)$ is a 2×6 matrix.

Let $\xi_1=-0.5$ and $\xi_2=0.5$ denote the values of the nondimensional coordinates at local nodes j ($j=1,2$) for each segment. Let U_j^m, W_j^m and $W_j'^m$, and F_{1j}^m, F_{3j}^m and M_j^m ($j=1,2$, $m=1-N$) denote the values of nondimensional generalized displacements U, W and $W_{,\xi}$, and the values of generalized forces F_1, F_3, and M, respectively, at local nodes j ($j=1,2$) for segment m.

From Eqs. (34) and (42), the generalized displacement vector $\mathbf{U}_j^m=\{U_j^m\quad W_j^m\quad W_j'^m\}$ may be expressed as

$$\mathbf{U}_j^m=\{U_j^m\quad W_j^m\quad W_j'^m\}=\mathbf{N}_{uj}^m\mathbf{C}^m \tag{45}$$

$$\mathbf{N}_{uj}^m=\begin{bmatrix}\mathbf{e}_1^t\mathbf{E}(\xi_j)\\ \mathbf{e}_2^t\mathbf{E}(\xi_j)\\ \mathbf{e}_2^t\mathbf{E}'(\xi_j)\end{bmatrix} \tag{46}$$

where $\mathbf{N}_{uj}^m$ is a 3×6 matrix, $j=1,2$, $m=1-N$, $\mathbf{C}^m$ is the column matrix of undetermined coefficients (Eq. (44)) corresponding segment m, $\mathbf{e}_1=\{1\quad 0\}$, $\mathbf{e}_2=\{0\quad 1\}$, $\mathbf{E}'=\mathbf{E}_{,\xi}$.

From Eqs. (11)–(13), (34) and (42), the generalized force vector $\mathbf{F}_j^m=\{F_{1j}^m\quad F_{3j}^m\quad M_j^m\}$ may be expressed as

$$\mathbf{F}_j^m=\{F_{1j}^m\quad F_{3j}^m\quad M_j^m\}=\mathbf{N}_{Fj}^m\mathbf{C}^m \tag{47}$$

$$\mathbf{N}_{Fj}^m=\begin{bmatrix}EA\mathbf{e}_1^t\mathbf{E}'(\xi_j)\\ \frac{EI}{l^2}\mathbf{e}_2^t[(\eta^2U_{s,\xi}(\xi_j)-K^2-k^2\cos^2\beta)\mathbf{E}'(\xi_j)-\mathbf{E}'''(\xi_j)]\\ \frac{EI}{l}\mathbf{e}_2^t\mathbf{E}''(\xi_j)\end{bmatrix} \tag{48}$$

where $\mathbf{N}_{Fj}^m$ is a 3×6 matrix, $j=1,2$, $m=1-N$, $\mathbf{E}'=\mathbf{E}_{,\xi}$, $\mathbf{E}''=\mathbf{E}_{,\xi\xi}$, $\mathbf{E}'''=\mathbf{E}_{,\xi\xi\xi}$.

From boundary conditions given in Eq. (16) and Eqs. (45) and (47), one may obtain

$$\mathbf{U}_1^1=\mathbf{N}_{u1}^1\mathbf{C}^1=\mathbf{0} \tag{49}$$

$$\mathbf{F}_2^N=\mathbf{N}_{F2}^N\mathbf{C}^N=\mathbf{0} \tag{50}$$

From the continuity conditions at common node between two adjacent segments, $\mathbf{U}_2^m=\mathbf{U}_1^{m+1}$ and $\mathbf{F}_2^m=\mathbf{F}_1^{m+1}$, and Eqs. (45) and (47), one may obtain

$$\mathbf{N}_{u2}^m\mathbf{C}^m-\mathbf{N}_{u1}^{m+1}\mathbf{C}^{m+1}=\mathbf{0} \tag{51}$$

$$\mathbf{N}_{F2}^m\mathbf{C}^m-\mathbf{N}_{F1}^{m+1}\mathbf{C}^{m+1}=\mathbf{0} \tag{52}$$

where $m=1,\ldots,N-1$.

From Eqs. (49)–(52), one may obtain a set of homogeneous equations expressed by

$$\mathbf{K}(K)\mathbf{C}_G=\mathbf{0} \tag{53}$$

$$\mathbf{K}(K)=\begin{bmatrix}\mathbf{N}_{u1}^1 & & & & & & & & \\ \mathbf{N}_{u2}^1 & -\mathbf{N}_{u1}^2 & & & & & & & \\ \mathbf{N}_{F2}^1 & -\mathbf{N}_{F1}^2 & & & & & & & \\ & \mathbf{N}_{u2}^2 & -\mathbf{N}_{u1}^3 & & & & & & \\ & \mathbf{N}_{F2}^2 & -\mathbf{N}_{F1}^3 & & & & & & \\ & & \mathbf{N}_{u2}^3 & & & & & & \\ & & \mathbf{N}_{F2}^3 & & & & & & \\ & & & \ddots & & & & & \\ & & & & -\mathbf{N}_{u1}^{N-1} & & & & \\ & & & & -\mathbf{N}_{F1}^{N-1} & & & & \\ & & & & \mathbf{N}_{u2}^{N-1} & -\mathbf{N}_{u1}^N & & & \\ & & & & \mathbf{N}_{F2}^{N-1} & -\mathbf{N}_{F1}^N & & & \\ & & & & & \mathbf{N}_{F2}^N & & & \end{bmatrix} \tag{54}$$

$$\mathbf{C}_G=\{\mathbf{C}^1\quad \mathbf{C}^2\quad \mathbf{C}^3\quad \cdots\quad \mathbf{C}^N\} \tag{55}$$

where $\mathbf{K}(K)$ denotes $\mathbf{K}$ is a function of K defined in Eq. (30), $\mathbf{K}$ is a $6N\times 6N$ matrix, and $\mathbf{C}_G$ is a column matrix of order $6N\times 1$ assembled from the column matrix $\mathbf{C}^m$ ($m=1-N$).

For a nontrivial $\mathbf{C}_G$, the determinant of the matrix $\mathbf{K}$ must be equal to zero. The values of K which make the determinant vanish are called eigenvalues of matrix $\mathbf{K}$ and give the natural frequencies of the rotating Euler beam through $\overline{K}$ defined in Eq. (31). The bisection method is used here to find the eigenvalues.

3. Numerical examples

In order to investigate the effect of the number of segments and precision used in computation on the convergence rate of solution and accuracy of the natural frequency for very slender rotating beam at very high angular velocity, the following cases are considered: slenderness ratio $\bar{\eta} = 1000$, setting angle $\beta = 0°$, dimensionless radius of the rotating hub $\bar{r} = 1,\ 1.5$, dimensionless angular velocity $\bar{k} = 0.06$ and number of segments $N = 1, 2, 3, 5$. Computation is in double precision for all cases. However, quadruple precision is also used for the cases with $N = 1$. The maximum steady state axial strains (Eq. (21)) corresponding to $\bar{r} = 1$ and 1.5 at $\bar{k} = 0.06$ are $\varepsilon_{\max} = 5.4 \times 10^{-3}$ and 7.2×10^{-3}, respectively. Thus, $\bar{k} = 0.06$ may be regarded as a very high angular velocity for $\bar{r} = 1$ and 1.5. Let $\overline{K}_i$ denote the ith dimensionless natural frequency of the rotating beam. The results are shown in Table 1. It can be seen that the convergence rate of the power series is nearly the same for all frequencies, and the number of terms used in the power series decrease with increase in the number of segments. It is found that the higher frequencies are not obtained for the cases using one segment and double precision, and except the natural frequencies obtained using one segment and double precision, the natural frequencies obtained for the rest cases are identical to six digits. It is clear that by subdividing the rotating beam into several segments, one can not only increase the rate of convergence of the power series but also improve the accuracy of the natural frequency calculated with the same precision. It seems that double precision used in the computation is sufficient to obtain accurate natural frequency of rotating slender beam at very high rotation speed. It can be seen that the number of terms used in the power series decrease with increase in the number of segments. To explore a possible explanation for the accuracy lost of natural frequencies for the cases using one segment and double precision, the determinant of matrix **K** (Eq. (53)) as a function of the dimensionless frequency $\overline{K}$ calculated with double and quadruple precision are depicted in Fig. 4 for the case with $N = 1$ and $\bar{r} = 1.5$. It may be noted that the curve calculated in double precision is fluctuated around the smooth curve calculated in quadruple precision. The fluctuation of the curve may be a typical symptom of accuracy lost due to insufficient precision in computation. It seems that the accuracy of solution may be improved with increase in computation precision.

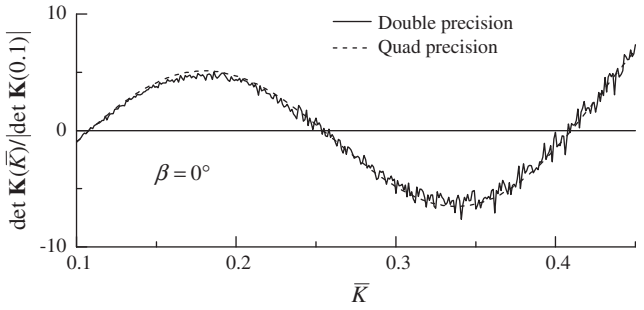

Fig. 4. Determinant of matrix **K** (Eq. (53)) verse the dimensionless frequency $\overline{K}$.

In the rest of the section, we subdivide the rotating beam in to three segments and use double precision in computation for all examples studied.

To investigate the effect of Coriolis force and rotary inertia on the natural frequency of rotating Euler beams, several numerical examples are studied. Here the following cases are considered:

Ea – All the terms in Eq. (25) are considered.
Eb – The Coriolis force terms (single underlined terms in Eq. (25)) are not considered.
Ec – The rotary inertia terms (double underlined terms in Eq. (25)) are not considered.
Ed – The Coriolis force terms and rotary inertia terms are not considered.

The examples considered are: slenderness ratio $\bar{\eta} = 20,\ 50,\ 100$, setting angle $\beta = 90°$, dimensionless radius of the rotating hub $\bar{r} = 0$, and dimensionless angular velocity

Table 1
Comparison of results for different numbers of segment ($\beta = 0°$, $\bar{\eta} = 1000$, $\bar{k} = 0.06$).

$\bar{r}$	i	$\overline{K}_i^1$	I_1	$\overline{K}_i^{1*}$, $\overline{K}_i^2$, $\overline{K}_i^3$, $\overline{K}_i^5$	I_1^*	I_2	I_3	I_5
1	1	0.095034	120	0.095036	120	69	54	41
	2	0.225414	119	0.225399	119	68	54	42
	3	0.364765	118	0.364733	118	69	54	42
	4	0.520978	120	0.520947	120	71	56	44
	5	0.693584	117	0.693418	117	69	55	42
	6	0.879911	116	0.879799	116	69	54	42
	7	1.07900	115	1.07898	115	69	54	42
	8	1.29057	115	1.29076	115	69	54	42
	9	1.51306	114	1.51533	114	69	54	42
	10	–	–	1.56965	114	69	55	42
	11	–	–	1.75312	114	69	55	42
	12	–	–	2.00459	114	69	55	42
1.5	1	0.108115	135	0.107975	135	75	58	44
	2	0.253961	133	0.254346	133	75	58	45
	3	–	–	0.409829	133	75	59	45
	4	–	–	0.582687	133	76	60	46
	5	–	–	0.772541	132	77	60	46
	6	–	–	0.976737	131	76	59	45
	7	–	–	1.19381	130	75	59	45
	8	–	–	1.42330	129	75	59	45
	9	–	–	1.56965	128	75	59	45
	10	–	–	1.66523	128	75	59	45
	11	–	–	1.91986	128	75	59	45
	12	–	–	2.18758	127	76	59	45

$\overline{K}_i^N$, ($N = 1, 2, 3, 5$) denote that $\overline{K}_i$ are obtained using N segments and double precision, and I_N denote the corresponding number of terms used in the power series.
$\overline{K}_i^{1*}$ denotes that $\overline{K}_i$ are obtained using one segment and quadruple precision, and I_1^* denotes the corresponding number of terms used in the power series.
The symbol "–" denotes that erroneous solution or no converged solution is obtained.

Table 2
Comparison of results for different cases ($\beta = 90°$, $\bar{r} = 0$, $N = 3$).

$\bar{\eta}$	$\bar{k}$	Case	$\overline{K}_1$	$\overline{K}_2$	$\overline{K}_3$	$\overline{K}_4$	$\overline{K}_5$
20	0	Ea	0.17479	1.05953	1.57080(a)	2.82431	4.71239(a)
		Eb	0.17479	1.05953	1.57080(a)	2.82431	4.71239(a)
		Ec	0.17580	1.10172	1.57080(a)	3.08486	4.71239(a)
		Ed	0.17580	1.10172	1.57080(a)	3.08486	4.71239(a)
		T[a]	0.17182	0.95696	1.57080(a)	2.33755	4.71239(a)
	0.1	Ea	0.17871	1.08105	1.58112(a)	2.84767	4.71573(a)
		Eb	0.18006	1.08303	1.56761(a)	2.84892	4.71133(a)
		Ec	0.17972	1.12413	1.58132(a)	3.11043	4.71617(a)
		Ed	0.18109	1.12632	1.56761(a)	3.11205	4.71133(a)
		T[a]	0.17530	0.98084	1.58090(a)	2.36838	4.71565(a)
50	0	Ea	0.07026	0.43786	1.21530	1.57080(a)	2.35176
		Eb	0.07026	0.43786	1.21530	1.57080(a)	2.35176
		Ec	0.07032	0.44069	1.23394	1.57080(a)	2.41804
		Ed	0.07032	0.44069	1.23394	1.57080(a)	2.41804
		T[a]	0.07006	0.42956	1.16396	1.57080(a)	2.18360
	0.1	Ea	0.08079	0.49511	1.27989	1.58044(a)	2.42053
		Eb	0.08141	0.49574	1.28048	1.56761(a)	2.42096
		Ec	0.08086	0.49836	1.29965	1.58046(a)	2.48885
		Ed	0.08148	0.49900	1.30026	1.56761(a)	2.48932
		T[a]	0.08033	0.48736	1.23102	1.58042(a)	2.25797
100	0	Ea	0.03515	0.21999	0.61460	1.20047	1.57080(a)
		Eb	0.03515	0.21999	0.61460	1.20047	1.57080(a)
		Ec	0.03516	0.22034	0.61697	1.20902	1.57080(a)
		Ed	0.03516	0.22034	0.61697	1.20902	1.57080(a)
		T[a]	0.03513	0.21891	0.60755	1.17564	1.57080(a)
	0.1	Ea	0.05009	0.32030	0.73655	1.33525	1.58038(a)
		Eb	0.05048	0.32065	0.73685	1.33554	1.56761(a)
		Ec	0.05010	0.32084	0.73946	1.34483	1.58039(a)
		Ed	0.05049	0.32120	0.73977	1.34513	1.56761(a)
		T[a]	0.04987	0.31932	0.73034	1.31266	1.58037(a)

[a] The results of Timoshenko beam are obtained using the method and data given in [15].

$\bar{k} = 0,\ 0.1$. The maximum steady state axial strain (Eq. (21)) corresponding to $\bar{k} = 0.1$ is $\varepsilon_{max} = 5 \times 10^{-3}$. Thus, $\bar{k} = 0.1$ may be regarded as a very high angular velocity for $\bar{r} = 0$.

The lowest five natural frequencies of the present study and the results of Timoshenko beam obtained by the authors using the method and data given in [15] are shown in Table 2. The natural frequency corresponding to the fourth lateral vibration mode for rotating beams with slenderness ratio $\bar{\eta} = 20$ and 50 is depicted in Fig. 5. With the consideration of the Coriolis force, except $\beta = 0$ or $\bar{k} = 0$, the axial and lateral vibrations are coupled in the vibration modes. In Table 2, "(a)" denotes that the corresponding vibration mode is axial vibration at $\bar{k} = 0$ and is dominated by axial vibration at $\bar{k} \neq 0$. From Table 2 and Fig. 5, it can be seen that for higher natural frequencies of lateral vibration, the discrepancy between the results of Ea and Ec increases with decrease of the slenderness ratio. It seems that the effect of the rotary inertia on the higher natural frequencies of the Euler beam is not negligible when the slenderness ratio is small. The discrepancy between the results of Timoshenko beam and Euler beam increases for higher natural frequencies of lateral vibration with decrease of the slenderness ratio. It indicates that the effect of the shear deformation on the natural frequencies of beam is not negligible when the slenderness ratio is small. The difference between the results of Ea and Eb (Ec and Ed) is still small for all slenderness ratios at high angular velocity. It seems that the effect of the Coriolis force on the natural frequencies of the rotating Euler beam may be negligible in practice.

To investigate the effect of Coriolis force and centrifugal stiffening on the coupling of the axial and lateral vibration modes, the following case is considered: $\beta = 90°$, $\bar{r} = 1$ and $\bar{\eta} = 78$. Fig. 6 shows

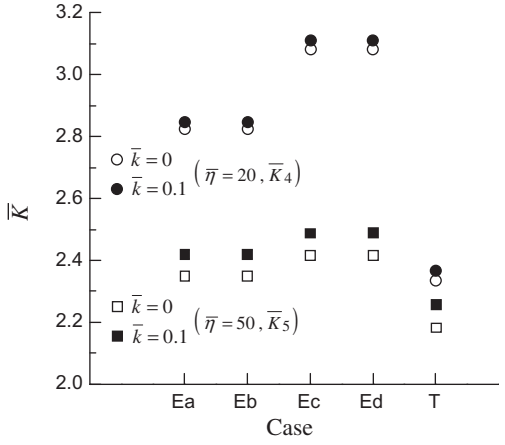

Fig. 5. The dimensionless natural frequency corresponding to the fourth lateral vibration mode.

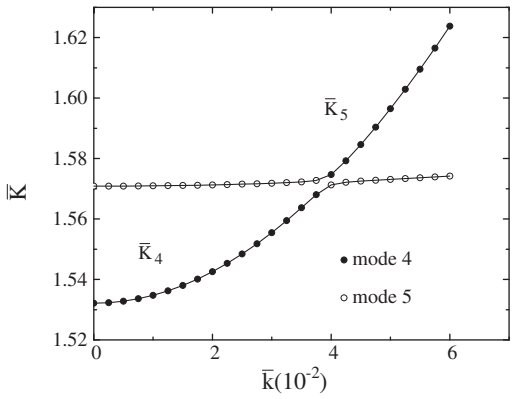

Fig. 6. The fourth and fifth natural frequencies verse the dimensionless frequency $\overline{K}$ ($\beta = 90°$, $r = 1$, $\eta = 78$).

the fourth and the fifth dimensionless natural frequencies for the rotating beam considered at different dimensionless angular velocities. Let mode 4 denote the fourth bending vibration mode at $\bar{k} = 0$ and the vibration mode dominated by the fourth bending vibration mode at $\bar{k} \neq 0$. Let mode 5 denote the first axial vibration mode at $\bar{k} = 0$ and the vibration mode dominated by the first axial vibration mode at $\bar{k} \neq 0$. Fig. 7 shows how mode 4 and mode 5 change with the dimensionless angular velocities. It can be seen from Fig. 6 that when the beam is stationary, the fourth and the fifth natural frequencies are relatively close, and their modes are mode 4 mode 5, respectively. Because the fourth frequency tend to increase at a faster rate than that of the fifth frequency, the phenomenon known as frequency veering [24] is observed. From the natural frequencies in Fig. 6 and the mode shapes in Fig. 7 we can see that at $\bar{k} = 0.05$ modes corresponding to the fourth and the fifth natural frequency have switched, i.e., the mode of the fourth frequency is mode 5 and the mode of the fifth frequency is mode 4. In the veering region, for example, $\bar{k} = 0.04$, both modes are strongly coupled.

To investigate the effect of angular velocity on the natural frequency of rotating Euler beams with different slenderness ratios, the following cases are considered: dimensionless angular velocity $\bar{k} = 0,\ 0.01,\ 0.03,\ 0.06$, slenderness ratio $\bar{\eta} = 20,\ 50,\ 100,\ 500,\ 1000$, setting angle $\beta = 0°, 90°$, and dimensionless radius of the rotating hub $\bar{r} = 0,\ 0.5,\ 1,\ 1.5$. The first dimensionless natural frequency for rotating beam with different slenderness ration and $\bar{r} = 1.5$ at different $\bar{k}$ is depicted in Fig. 8. The first six dimensionless natural frequencies for different $\bar{r}$ and some results available in [7] are tabulated in Tables 3–6. In Tables 3–6, "(a)" denotes that the corresponding vibration mode is axial vibration at $\beta = 0°$ or $\bar{k} = 0$ and is dominated by axial vibration at $\beta = 90°$ and $\bar{k} \neq 0$. Duo to the stiffening effect of the centrifugal force, as expected, it can be seen from Fig. 8 and Tables 3–6 that the lower natural frequencies of lateral vibration increase remarked with increase of angular velocity and the hub radius for very slender beam. It is seen that the natural frequencies of flapwise bending vibrations ($\beta = 0°$) are always higher than those of lagwise bending vibrations ($\beta = 90°$). However, their difference becomes much smaller for higher mode. It may be noted that for $\beta = 0°$, the natural frequencies of axial vibration slightly decrease with increase of angular velocity, but are independent of the radius of the rotating hub. It can be seen from Eq. (25) that the axial vibration and the flapping vibration are not coupled and can be solved independently at $\beta = 0°$. The closed form solution for the natural frequency of axial vibration at $\beta = 0°$ may be easily obtained from Eq. (25) and expressed as $\overline{K} = [(n\pi + 0.5\pi)^2 - \bar{k}^2]^{1/2},\ n = 0, 1, 2, \ldots$ The values of the closed form solutions and the results given in Tables 3–6 are identical. It may also be noted that for $\beta = 90°$, the dimensionless natural frequencies of axial vibration slightly increase with increase of angular velocity and the radius of the rotating hub, but slightly decrease with increase of slenderness ratio of the rotating beam. The decrease of the dimensionless natural frequencies of axial vibration may be caused by the centripetal term $\Omega^2 U$ in Eq. (30). In this section it is mentioned that $\bar{k} = 0.1$ may be regarded as a very high angular velocity for $\bar{r} = 0$. Thus, the centripetal effect on the dimensionless natural frequencies of axial vibration of rotating beam may be negligible in practice.

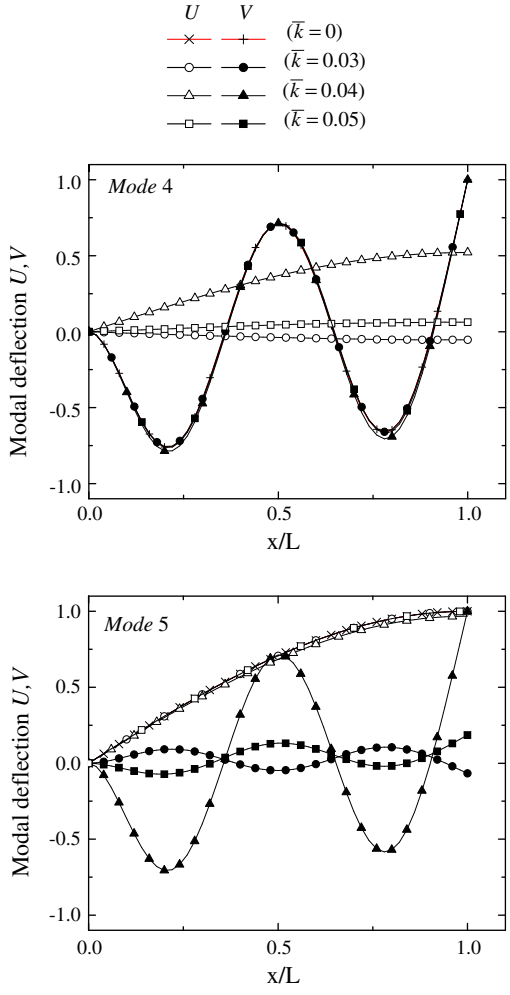

Fig. 7. Mode 4 and mode 5 at different dimensionless frequencies $\overline{K}$ ($\beta = 90°$, $r = 1$, $\eta = 78$).

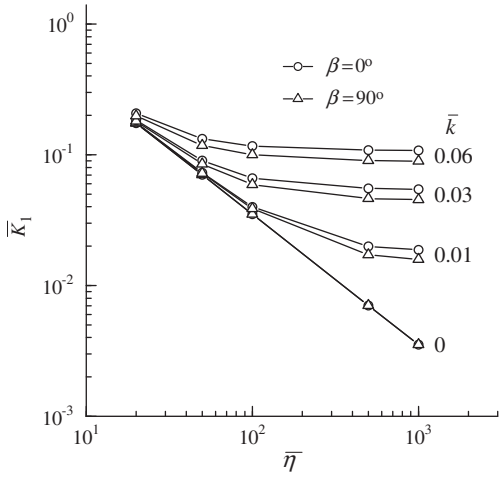

Fig. 8. The first dimensionless natural frequency for rotating beam ($\bar{r} = 1.5$).

4. Conclusions

In this paper, the correct governing equations for linear vibration of a rotating Euler beam are derived. The natural frequencies of flapwise bending vibration, and coupled lagwise bending and axial vibration are investigated for the rotating Euler beam. A practical method based on the power series solution is proposed to solve the natural frequency of slender rotating beam at very high angular velocity using double precision computation. The rotating beam is subdivided into several segments. Two coupled governing equations for linear vibration of each segment are solved by a power series with six independent coefficients. Substituting the

Table 3
Dimensionless frequencies for rotating beam with different slenderness ratios ($\bar{r} = 0$, $N = 3$).

β	$\bar{k}$	$\bar{\eta}$	$\overline{K}_1$	$\overline{K}_2$	$\overline{K}_3$	$\overline{K}_4$	$\overline{K}_5$	$\overline{K}_6$
0°	0	20	0.17479	1.05953	1.57080(a)	2.82431	4.71239(a)	5.19119
		50	0.07026	0.43786	1.21530	1.57080(a)	2.35176	3.82644
		100	0.03515	0.21999	0.61460	1.20047	1.57080(a)	1.97618
		500	0.00703	0.04407	0.12338	0.24173	0.39954	0.59671
		1000	0.00352	0.02203	0.06169	0.12089	0.19984	0.29851
	0.01	20	0.17512	1.05982	1.57076(a)	2.82458	4.71238(a)	5.19144
		50	0.07110	0.43859	1.21601	1.57076(a)	2.35248	3.82717
		100	0.03681	0.22145	0.61604	1.20195	1.57076(a)	1.97768
		500	0.01290	0.05089	0.13039	0.24906	0.40706	0.60437
		1000	0.01120	0.03364	0.07465	0.13487	0.21444	0.31350
	0.03	20	0.17778	1.06206	1.57051(a)	2.82668	4.71229(a)	5.19348
		50	0.07749	0.44438	1.22168	1.57051(a)	2.35826	3.83298
		100	0.04796	0.23282	0.62742	1.21371	1.57051(a)	1.98966
		500	0.03228	0.08787	0.17586	0.30051	0.46227	0.66201
		1000	0.03109	0.07847	0.13761	0.21290	0.30413	0.41188
	0.06	20	0.18645	1.06960	1.56965(a)	2.83375	4.71201(a)	5.20036
		50	0.09583	0.46338	1.24062	1.56965(a)	2.37766	3.85252
		100	0.07358	0.26765	0.66425	1.25247	1.56965(a)	2.02949
		500	0.06219	0.15692	0.27518	0.42570	0.60804	0.82334
		1000	0.06108	0.15072	0.24802	0.36025	0.48701	0.62736
90°	0.01	20	0.17483	1.05976	1.57090(a)	2.82455	4.71242(a)	5.19143
		50	0.07039	0.43847	1.21597	1.57089(a)	2.35246	3.82715
		100	0.03542	0.22122	0.61596	1.20191	1.57089(a)	1.97766
		500	0.00815	0.04990	0.13001	0.24886	0.40694	0.60428
		1000	0.00505	0.03212	0.07397	0.13450	0.21420	0.31334
		1000[7]	0.00505	0.03212	–	-	-	-
	0.03	20	0.17517	1.06152	1.57173(a)	2.82646	4.71269(a)	5.19335
		50	0.07142	0.44333	1.22129	1.57166(a)	2.35806	3.83284
		100	0.03740	0.23087	0.62669	1.21333	1.57166(a)	1.98942
		500	0.01192	0.08258	0.17328	0.29900	0.46129	0.66132
		1000	0.00817	0.07250	0.13429	0.21077	0.30264	0.41078
	0.06	20	0.17629	1.06746	1.57452(a)	2.83288	4.71359(a)	5.19984
		50	0.07461	0.45936	1.23905	1.57427(a)	2.37684	3.85195
		100	0.04251	0.26077	0.66148	1.25097	1.57425(a)	2.02856
		500	0.01631	0.14495	0.26853	0.42142	0.60506	0.82114
		1000	0.01138	0.13822	0.24063	0.35519	0.48328	0.62447

Table 4
Dimensionless frequencies for rotating beam with different slenderness ratios ($\bar{r} = 0.5$, $N = 3$).

β	$\bar{k}$	$\bar{\eta}$	$\overline{K}_1$	$\overline{K}_2$	$\overline{K}_3$	$\overline{K}_4$	$\overline{K}_5$	$\overline{K}_6$
0°	0.01	20	0.17535	1.06001	1.57076(a)	2.82476	4.71238(a)	5.19163
		50	0.07165	0.43907	1.21651	1.57076(a)	2.35300	3.82769
		100	0.03786	0.22242	0.61704	1.20301	1.57076(a)	1.97877
		500	0.01560	0.05495	0.13504	0.25413	0.41239	0.60986
		1000	0.01417	0.03941	0.08229	0.14385	0.22426	0.32389
	0.03	20	0.17974	1.06377	1.57051(a)	2.82834	4.71229(a)	5.19514
		50	0.08191	0.44868	1.22613	1.57051(a)	2.36290	3.83770
		100	0.05477	0.24099	0.63621	1.22305	1.57051(a)	1.99933
		500	0.04141	0.10696	0.20338	0.33491	0.50166	0.70490
		1000	0.04043	0.09877	0.16906	0.25554	0.35715	0.47391
	0.06	20	0.19384	1.07636	1.56965(a)	2.84040	4.71201(a)	5.20697
		50	0.10946	0.47966	1.25799	1.56965(a)	2.39597	3.87125
		100	0.09036	0.29495	0.69649	1.28804	1.56965(a)	2.06696
		500	0.08087	0.19752	0.33807	0.51095	0.71403	0.94734
		1000	0.07997	0.19196	0.31256	0.44930	0.60145	0.76716
90°	0.01	20	0.17505	1.05995	1.57090(a)	2.82474	4.71242(a)	5.19161
		50	0.07094	0.43896	1.21646	1.57089(a)	2.35298	3.82768
		100	0.03651	0.22220	0.61696	1.20296	1.57089(a)	1.97874
		500	0.01197	0.05403	0.13467	0.25394	0.41226	0.60978
		1000	0.01004	0.03812	0.08168	0.14350	0.22404	0.32373
	0.03	20	0.17716	1.06323	1.57173(a)	2.82813	4.71269(a)	5.19501
		50	0.07618	0.44765	1.22573	1.57167(a)	2.36270	3.83756
		100	0.04580	0.23910	0.63548	1.22267	1.57166(a)	1.99909
		500	0.02853	0.10266	0.20115	0.33356	0.50076	0.70425
		1000	0.02709	0.09409	0.16637	0.25376	0.35588	0.47296
	0.06	20	0.18404	1.07422	1.57453(a)	2.83952	4.71359(a)	5.20644
		50	0.09137	0.47576	1.25643	1.57428(a)	2.39515	3.87068
		100	0.06740	0.28870	0.69384	1.28658	1.57426(a)	2.06605
		500	0.05406	0.18812	0.33266	0.50738	0.71148	0.94541
		1000	0.05272	0.18228	0.30671	0.44525	0.59843	0.76479

Table 5
Dimensionless frequencies for rotating beam with different slenderness ratios ($\bar{r} = 1.0$, $N = 3$).

β	$\bar{k}$	$\bar{\eta}$	$\overline{K}_1$	$\overline{K}_2$	$\overline{K}_3$	$\overline{K}_4$	$\overline{K}_5$	$\overline{K}_6$
0°	0.01	20	0.17557	1.06020	1.57076(a)	2.82495	4.71238(a)	5.19181
		50	0.07219	0.43956	1.21700	1.57076(a)	2.35352	3.82822
		100	0.03888	0.22339	0.61805	1.20406	1.57076(a)	1.97985
		500	0.01788	0.05870	0.13950	0.25909	0.41763	0.61530
		1000	0.01661	0.04437	0.08915	0.15217	0.23358	0.33387
	0.03	20	0.18169	1.06547	1.57051(a)	2.83001	4.71229(a)	5.19679
		50	0.08609	0.45294	1.23056	1.57051(a)	2.36753	3.84241
		100	0.06080	0.24888	0.64484	1.23231	1.57051(a)	2.00894
		500	0.04882	0.12287	0.22694	0.36528	0.53741	0.74468
		1000	0.04793	0.11532	0.19472	0.29058	0.40138	0.52663
	0.06	20	0.20094	1.08307	1.56965	2.84703	4.71201	5.21357
		50	0.12153	0.49536	1.27507	1.56965	2.41411	3.88986
		100	0.10442	0.31976	0.72703	1.32243	1.56965	2.10361
		500	0.09585	0.23062	0.38939	0.58102	0.80246	1.05271
		1000	0.09504	0.22540	0.36473	0.52095	0.69342	0.87980
90°	0.01	20	0.17528	1.06014	1.57090(a)	2.82492	4.71242(a)	5.19180
		50	0.07149	0.43944	1.21696	1.57089(a)	2.35349	3.82820
		100	0.03757	0.22316	0.61796	1.20402	1.57089(a)	1.97983
		500	0.01482	0.05784	0.13914	0.25889	0.41751	0.61521
		1000	0.01326	0.04323	0.08859	0.15184	0.23336	0.33372
		1000[7]	0.01326	0.04324	–	–	–	–
	0.03	20	0.17913	1.06493	1.57173(a)	2.82979	4.71269(a)	5.19666
		50	0.08066	0.45192	1.23016	1.57167(a)	2.36732	3.84227
		100	0.05286	0.24704	0.64413	1.23193	1.57166(a)	2.00871
		500	0.03849	0.11914	0.22494	0.36404	0.53657	0.74407
		1000	0.03735	0.11134	0.19239	0.28902	0.40025	0.52578
	0.06	20	0.19147	1.08093	1.57454(a)	2.84615	4.71359(a)	5.21304
		50	0.10546	0.49158	1.27353	1.57429(a)	2.41330	3.88930
		100	0.08524	0.31398	0.72448	1.32100	1.57426(a)	2.10271
		500	0.07454	0.22260	0.38469	0.57787	0.80018	1.05098
		1000	0.07349	0.21719	0.35972	0.51744	0.69079	0.87773

Table 6
Dimensionless frequencies for rotating beam with different slenderness ratios ($\bar{r} = 1.5$, $N = 3$).

β	$\bar{k}$	$\bar{\eta}$	$\overline{K}_1$	$\overline{K}_2$	$\overline{K}_3$	$\overline{K}_4$	$\overline{K}_5$	$\overline{K}_6$
0°	0.01	20	0.17579	1.06039	1.57076(a)	2.82513	4.71238(a)	5.19199
		50	0.07273	0.44005	1.21750	1.57076(a)	2.35403	3.82874
		100	0.03987	0.22435	0.61905	1.20511	1.57076(a)	1.98093
		500	0.01990	0.06221	0.14380	0.26392	0.42280	0.62067
		1000	0.01872	0.04878	0.09542	0.15995	0.24244	0.34349
	0.03	20	0.18361	1.06717	1.57051(a)	2.83168	4.71229(a)	5.19845
		50	0.09008	0.45716	1.23496	1.57051(a)	2.37214	3.84712
		100	0.06628	0.25650	0.65335	1.24149	1.57051(a)	2.01849
		500	0.05522	0.13680	0.24784	0.39270	0.57031	0.78188
		1000	0.05438	0.12967	0.21697	0.32102	0.44004	0.57314
	0.06	20	0.20780	1.08974	1.56965(a)	2.85364	4.71201(a)	5.22015
		50	0.13248	0.51055	1.29188	1.56965(a)	2.43209	3.90837
		100	0.11675	0.34262	0.75609	1.35575	1.56965(a)	2.13949
		500	0.10875	0.25933	0.43388	0.64187	0.87974	1.14567
		1000	0.10798	0.25435	0.40983	0.58269	0.77254	0.97674
90°	0.01	20	0.17550	1.06033	1.57090(a)	2.82511	4.71242(a)	5.19198
		50	0.07204	0.43993	1.21746	1.57089(a)	2.35401	3.82873
		100	0.03860	0.22413	0.61896	1.20507	1.57089(a)	1.98091
		500	0.01720	0.06141	0.14345	0.26373	0.42268	0.62059
		1000	0.01582	0.04775	0.09490	0.15964	0.24224	0.34335
	0.03	20	0.18108	1.06663	1.57173(a)	2.83146	4.71269(a)	5.19832
		50	0.08490	0.45614	1.23457	1.57167(a)	2.37194	3.84698
		100	0.05907	0.25472	0.65265	1.24111	1.57166(a)	2.01826
		500	0.04632	0.13345	0.24601	0.39155	0.56952	0.78130
		1000	0.04532	0.12614	0.21488	0.31961	0.43901	0.57235
	0.06	20	0.19862	1.08760	1.57455(a)	2.85276	4.71360(a)	5.21962
		50	0.11784	0.50687	1.29036	1.57429(a)	2.43127	3.90780
		100	0.09989	0.33722	0.75363	1.35435	1.57427(a)	2.13860
		500	0.09045	0.25220	0.42965	0.63902	0.87766	1.14407
		1000	0.08952	0.24708	0.40536	0.57955	0.77017	0.97486

power series solution of each segment into the corresponding boundary conditions at two end nodes of the rotating beam and the continuity conditions at common node between two adjacent segments, a set of homogeneous equations can be obtained. The natural frequencies may be determined by solving the homogeneous equations using the bisection method.

The effect of the number of segments on the convergence rate of solution and accuracy of the natural frequency for very slender rotating beam at very high angular velocity are investigated using numerical examples. It is demonstrated that the accuracy of solution and the rate of convergence of the power series solution can be improved with increase in the number of segments. The rotating beam is subdivided into three segments and double precision in computation is used for all examples studied. Due to effect of the Coriolis force and centrifugal stiffening, frequency veering phenomenon is observed when two natural frequencies corresponding to axial vibration and lateral vibration are close. Duo to the effect of the centrifugal stiffening, the lower natural frequencies of lateral vibration increase remarked with increase of angular velocity and the hub radius for very slender beam.

Finally, it may be emphasized that, although the proposed method are only applied to the uniform rotating cantilever beams here, the present method can be easily extended to non-uniform rotating beams with discontinuities, as well as with other end conditions.

Appendix A. Derivations and explicit forms of $\delta\varepsilon$, $\delta\mathbf{r}$, and $\ddot{\mathbf{r}}$

From Eqs. (3) and (5), using the approximation $\theta \approx w_{,x}$, and retaining all terms up to the first order of infinitesimal quantities, $\delta\mathbf{r}$ and $\delta\varepsilon$ may be approximated by

$$\delta\mathbf{r} = \{\, \delta\bar{u} - z\delta w_{,x} \quad 0 \quad \delta w - z w_{,x}\delta w_{,x} \,\} \tag{A.1}$$

$$\delta\varepsilon = \delta\bar{u}_{,x} + w_{,x}\delta w_{,x} - z\delta w_{,xx} \tag{A.2}$$

The second time derivative of $\mathbf{r}$ in Eq. (3) may be expressed as

$$\ddot{\mathbf{r}} = \ddot{r}_i\mathbf{e}_i + 2\dot{r}_i\dot{\mathbf{e}}_i + r_i\ddot{\mathbf{e}}_i \tag{A.3}$$

$$\dot{\mathbf{e}}_i = \boldsymbol{\Omega}\times\mathbf{e}_i, \quad \ddot{\mathbf{e}}_i = \boldsymbol{\Omega}\times\dot{\mathbf{e}}_i \tag{A.4}$$

where $i = 1, 2, 3$ and $\boldsymbol{\Omega}$ is given in Eq. (1).

From Eqs. 1, 3, and A.4, using the approximation $\theta \approx w_{,x}$, $\ddot{\mathbf{r}}$ in Eq. (A.3) may be approximated by

$$\ddot{\mathbf{r}} = \left\{ \begin{array}{c} \ddot{u} - z\ddot{w}_{,x} + 2\Omega\dot{w}\sin\beta + \Omega^2[-(R + x + \bar{u}) + zw_{,x}] \\ 2\Omega(\dot{u} - z\dot{w}_{,x})\cos\beta\Omega^2 y\cos^2\beta + \Omega^2(z + w)\sin\beta\cos\beta \\ \ddot{w} + 2\Omega(-\dot{u} + z\dot{w}_{,x})\sin\beta + \Omega^2 y\sin\beta\cos\beta - \Omega^2(z + w)\sin^2\beta \end{array} \right\} \tag{A.5}$$

References

[1] Schilhansl MJ. Bending frequency of a rotating cantilever beam. ASME J Appl Mech 1958;25:28–30.
[2] Stafford RO, Giurgiutiu V. Semi-analytic methods for rotating Timoshenko beams. Int J Mech Sci 1975;17:719–27.
[3] Wang JTS, Mahrenholtz O, Bohm J. Extended Galerkin's method for rotating beam vibrations using Legendre polynomials. Solid Mech Arch 1976;1:341–65.
[4] Leissa A. Vibrational aspects of rotating turbomachinery blades. ASME Appl Mech Rev 1981;34:629–35.
[5] Hodges DH, Rutkowski MJ. Free-vibration analysis of rotating beams by a variable-order finite-element method. AIAA J 1981;19:1459–66.
[6] Wright AD, Smith CE, Thresher RW, Wang JLC. Vibration modes of centrifugally stiffened beams. ASME J Appl Mech 1982;49:197–202.
[7] Yokoyama T. Free vibration characteristics of rotating Timoshenko beam. Int J Mech Sci 1988;30:743–55.
[8] Yoo HH, Shin SH. Vibration analysis of rotating cantilever beams. J Sound Vib 1998;212:807–28.
[9] Lee SY, Kuo YH. Bending frequency of a rotating beam with an elastically restrained root. ASME J Appl Mech 1991;58:209–14.
[10] Du H, Lim MK, Liew KM. A power series solution for vibration of a rotating Timoshenko beam. J Sound Vib 1994;175:505–23.
[11] Naguleswaran S. Lateral vibration of a centrifugally tensioned uniform Euler–Bernoulli beam. J Sound Vib 1994;176:613–24.
[12] Naguleswaran S. Comments on "A power series solution for vibration of a rotating Timoshenko beam". J Sound Vib 1995;186:345–9.
[13] Naguleswaran S. Out-of-plane vibration of a uniform Euler–Bernouilli beam attached to the inside of a rotating rim. J Sound Vib 1997;200:63–81.
[14] Banerjee JR. Dynamic stiffness formulation and free vibration analysis of centrifugally stiffened Timoshenko beams. J Sound Vib 2001;247:97–115.
[15] Lin SC, Hsiao KM. Vibration analysis of rotating Timoshenko beam. J Sound Vib 2001;240:303–22.
[16] Banerjee JR, Su H. Development of a dynamic stiffness matrix for free vibration analysis of spinning beams. Comput Struct 2004;82:2189–97.
[17] Wang G, Wereley NM. Free vibration analysis of rotating blades with uniform tapers. AIAA J 2004;42:2429–37.
[18] Lee SY, Sheu JJ. Free vibrations of a rotating inclined beam. ASME J Appl Mech 2007;74:406–14.
[19] Banerjee JR, Su H. Dynamic stiffness formulation and free vibration analysis of a spinning composite beam. Comput Struct 2006;84:1208–14.
[20] Likins PW. Mathematical modeling of spinning elastic bodies for model analysis. AIAA J 1973;11:1251–8.
[21] Simo JC, Vu-Quac K. The role of non-linear theories in transient dynamic analysis of flexible structures. J Sound Vib 1987;119:487–508.
[22] Hsiao KM. Corotational total Lagrangian formulation for three-dimensional beam element. AIAA J 1992;30:797–804.
[23] Hsiao KM, Yang RT, Lee AC. A consistent finite element formulation for nonlinear dynamic analysis of planar beam. Int J Numer Methods Eng 1994;37:75–89.
[24] Marugabandhu P, Griffin JH. A reduced-order model for evaluating the effect of rotational speed on the natural frequencies and mode shapes of blades. Trans ASME J Eng Gas Turb Power 2003;125:772–6.
[25] Chung TJ. Continuum mechanics. Englewood Cliffs, NJ: Prentice-Hall; 1988.
[26] Malvern DJ. Introduction to the mechanics of the continuous medium. Englewood Cliffs, NJ: Prentice-Hall; 1969.